Infrared Circular Polarization Sensor for Sea-Skimming Missile Detection

by
T. W. Nee
S. F. Nee
Naval Aviation Science and Technology Office
E. J. Bevan
Theater Missile Defense Project Office

NOVEMBER 1998

19981208 001

**NAVAL AIR WARFARE CENTER WEAPONS DIVISION
CHINA LAKE, CA 93555-6100**

Naval Air Warfare Center Weapons Division

FOREWORD

The performance of an infrared passive polarization sensor for discrimination and tracking applications has been extensively studied. In this report we discuss the concept and feasibility of using a circular polarization sensor to detect a sea-skimming cruise missile in a solar corridor. For (1) shipboard sensor and (2) interceptor/helicopter board sensor, the circular polarization reflection-reflection signatures for a cylindrical target above water plane with both flat and rough sea surface are studied quantitatively.

This report is a reprint of *The 1998 National Fire Control Symposium Theater Air and Missile Defense, 3-6 August 1998, San Diego, Calif.*

Approved by
J. FISCHER, *Head*
Naval Aviation Science and Technology Office
29 October 1998

Released for publication by
K. HIGGINS
Director for Research and Engineering

Under authority of
RAND F. FISHER
RADM., U.S. Navy
Commander

NAWCWD Technical Publication 8410

REPORT DOCUMENTATION PAGE

Public reporting burden for this collection of information is estimated to average 1 hour per response, including the time for reviewing instructions, searching existing data sources, gathering and maintaining the data needed, and completing and reviewing the collection of information. Send comments regarding this burden estimate or any other aspect of this collection of information, including suggestions for reducing this burden, to Washington Headquarters Services, Directorate for Information Operations and Reports, 1215 Jefferson Davis Highway, Suite 1204, Arlington, VA 22202-4302, and to the Office of Management and Budget, Paperwork Reduction Project (0704-0188), Washington, DC 20503.

1. AGENCY USE ONLY *(Leave blank)*	2. REPORT DATE November 1998	3. REPORT TYPE AND DATES COVERED Final

4. TITLE AND SUBTITLE
Infrared Circular Polarization Sensor for
Sea-Skimming Missile Detection (U)

5. FUNDING NUMBERS
N0002498WRB0109
N0001498WX20041

6. AUTHOR(S)
T. W. Nee, S. F. Nee, and E. J. Bevan

7. PERFORMING ORGANIZATION NAME(S) AND ADDRESS(ES)
Naval Air Warfare Center Weapons Division
China Lake, CA

8. PERFORMING ORGANIZATION REPORT NUMBER
NAWCWD TP 8410

9. SPONSORING/MONITORING AGENCY NAME(S) AND ADDRESS(ES)
Naval Sea Systems Command (SEA-01T)
2531 Jefferson Davis Highway
Arlington, VA 22242-5160

Office of Naval Research
800 North Quincy St.
Arlington, VA 22217-5660

10. SPONSORING/MONITORING AGENCY REPORT NUMBER

11. SUPPLEMENTARY NOTES

12a. DISTRIBUTION/AVAILABILITY STATEMENT
Approved for public release; distribution is unlimited.

12b. DISTRIBUTION CODE

13. ABSTRACT *(Maximum 200 words)*

The performance of an infrared passive polarization sensor for discrimination and tracking applications has been extensively studied. In this report we discuss the concept and feasibility of using a circular polarization sensor to detect a sea-skimming cruise missile in a solar corridor. For (1) shipboard sensor and (2) interceptor/helicopter board sensor, the circular polarization reflection-reflection signatures for a cylindrical target above water plane with both flat and rough sea surface are studied quantitatively.

14. SUBJECT TERMS
Circular Polarization, MWIR, Sea-Skimming Missile, Emission, Reflection, Sea-Background, Acquisition Range, Cylindrical Target, Solar Corridor

15. NUMBER OF PAGES
22

16. PRICE CODE

17. SECURITY CLASSIFICATION OF REPORT UNCLASSIFIED	18. SECURITY CLASSIFICATION OF THIS PAGE UNCLASSIFIED	19. SECURITY CLASSIFICATION OF ABSTRACT UNCLASSIFIED	20. LIMITATION OF ABSTRACT SAR

CONTENTS

This page intentionally left blank.

INTRODUCTION

Either linear or circular polarization is a fundamental property of radiation and is a well understood phenomenon. The imaging profiles and signatures of man-made targets are polarization-dependent. Natural background-clutter and plume signatures are mostly unpolarized or have very different polarization characteristics from those of the targets. Based upon this fact, polarization-based imaging of targets in clutter and background has received increasing attention since it can provide more discrimination power than simple intensity imaging (Reference 1).

We have made a performance analysis of an infrared passive polarization sensor for discrimination applications. The results show the application feasibility for (1) target/debris/altitude control module (ACM) discrimination of Ballistic Missile Defense (BMD) using linear polarization and (2) detection of a sea-skimming missile in the presence of sea clutter and solar background using circular polarization (References 2 through 5). The application of linear polarization imaging for real-target/background discrimination and mines-target identification has also been demonstrated (References 1 and 6). The three Stokes parameters imager was demonstrated by a preliminary pixel-by-pixel mid-wave infrared (MWIR) linear-polarization imager (Reference 7).

These developments provide the application potential of using passive linear polarization sensor for BMD discrimination/tracking (References 5 and 8). For a sea-skimming missile in the solar corridor, the solar radiation reflected from the (1) sea surface and (2) missile surface would have a significant circular component. However, the background of solar radiation reflected from the sea would have a negligibly small circular component, which is zero for a flat water surface (Reference 4). These phenomena can be used to detect a sea-skimming missile in the presence of sea clutter and solar background. In this report, we include the effects of atmospheric absorption and the rough sea surface, which have been neglected in previous studies.

THEORY OF POLARIZATION SIGNATURES

Based upon the different polarization characteristics of objects in the scene, the polarization Stokes parameter Q-, U-, and V-images provide more target-clutter discrimination capability than the intensity-only I-image, the existing infrared technology (References 1 through 8). As shown in Figure 1, the polarization state of light from a target surface coming toward the observer can be completely described by Stokes parameters $\mathbf{S} = (S_0, S_1, S_2, S_3) = (I, Q, U, V)$. I is the total intensity; Q and U are the two component intensities of linear polarization radiation. V is the component related to circular polarization intensities. They satisfy the relations

$$I = I_{up} + I_p \tag{1}$$

and

$$I_p = \left(Q^2 + U^2 + V^2\right)^{1/2} \tag{2}$$

I_p and I_{up} are the intensities of polarized and unpolarized components respectively.
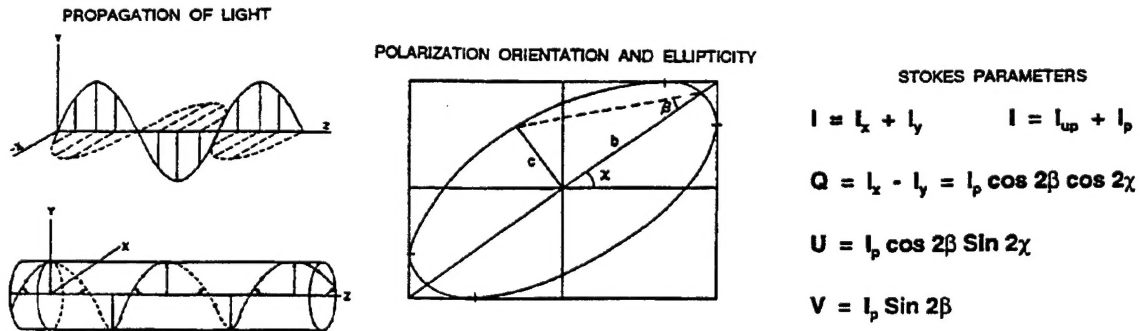
FIGURE 1. The Stokes Parameters Description of Electromagnetic Wave.

The radiation from the target toward the observer can be formulated as

$$\text{and} \quad \begin{pmatrix} I \\ Q \\ U \\ V \end{pmatrix} = \mathbf{M} \begin{pmatrix} I_o \\ Q_o \\ U_o \\ V_o \end{pmatrix} \tag{3}$$

where $\mathbf{M}$, the Mueller matrix, relates to the optical properties of the target surface, such as reflection, emission, and scattering. $\mathbf{S}_o = (I_o, Q_o, U_o, V_o)$ is the source radiation.

For the reflection from a smooth plane, as shown in Figure 2a, taking the x-y axis along the s- and p-wave polarization direction of the reflected beam, the reflection Mueller matrix is

$$
\mathbf{M_r} = R \begin{pmatrix} 1 & \cos 2\psi & 0 & 0 \\ \cos 2\psi & 1 & 0 & 0 \\ 0 & 0 & \sin 2\psi \cos \Delta & \sin 2\psi \sin \Delta \\ 0 & 0 & -\sin 2\psi \sin \Delta & \sin 2\psi \cos \Delta \end{pmatrix} \tag{4}
$$

where ψ and Δ are defined from

$$
\frac{r_p}{r_s} = \tan \psi \, e^{i\Delta} \tag{5}
$$

r_s and r_p are the complex reflection coefficients for s- and p-waves respectively. $R = (R_s + R_p)/2$ [$R_j = |r_j|^2$, j=s,p], is the reflectance. r_s, r_p, R and thus ψ and Δ are functions of the angle of incidence. Considering a smooth stainless-steel-like metal surface with optical constant (1.5 + i 4.5), the incident angle-dependent reflectance ψ and Δ are shown in Figure 3a. The two Mueller matrix elements M_{01} [= R cos 2ψ] and M_{23} [= R sin 2ψ sin Δ] are shown in Figure 3b. The two reflectances R_s and R_p are shown in Figure 3c.
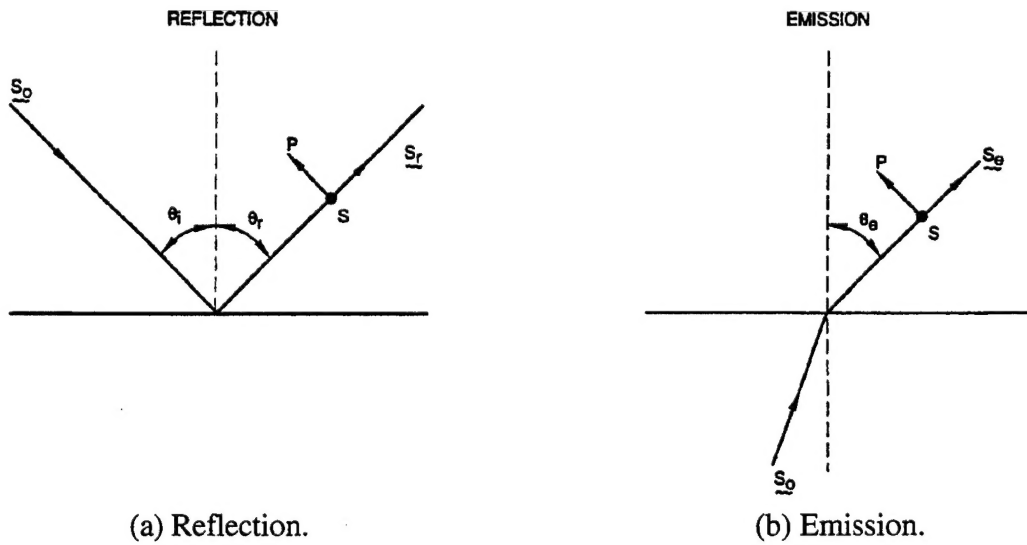

(a) Reflection.   (b) Emission.

FIGURE 2. The Reflection and Emission Geometry From a Plane.

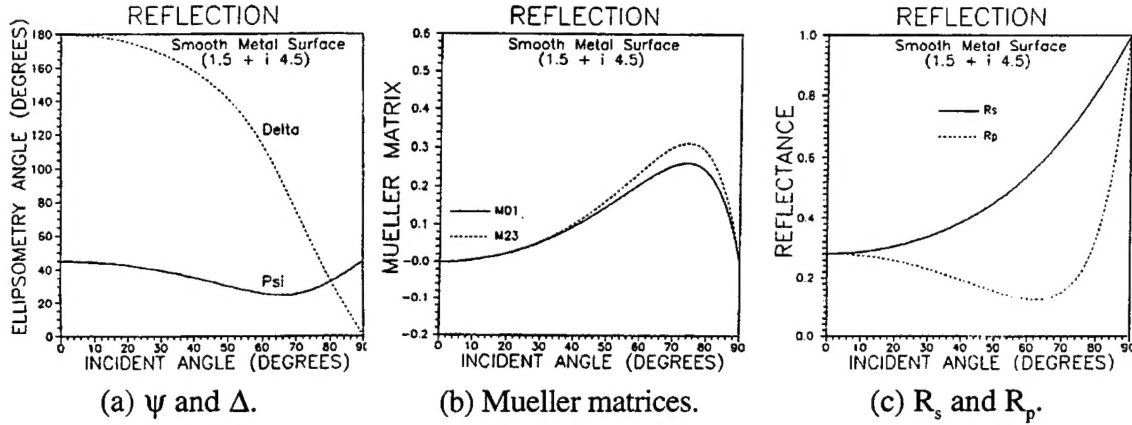(a) ψ and Δ. (b) Mueller matrices. (c) R_s and R_p.

FIGURE 3. The Calculated Reflection ψ, Δ, Mueller Matrix Elements and R_s, R_p for a Smooth Metal Plane of Optical Constants $1.5 + i\,4.5$.

For the emission case shown in Figure 2b, the ψ and Δ are defined from

$$\frac{t_p}{t_s} = \tan \psi \, e^{i\Delta} \tag{6}$$

t_s and t_p are the s- and p-wave complex transmission coefficients, for the radiation from the target interior below the surface. The emission Mueller matrix $\mathbf{M_e}$ has the same form as $\mathbf{M_r}$ in Equation 4, except R is replaced by $T = (T_s+T_p)/2$ $[T_j=|t_j|^2, j=s,p]$, the transmittance. t_s, t_p, T and thus ψ and Δ are functions of the angle of emission. For the smooth surface with optical constant $(1.5 + i\,4.5)$, the incident angle-dependent reflectance ψ and Δ are shown in Figure 4a. The two Mueller matrix elements M_{01} $[= T \cos 2\psi]$ and M_{23} $[= T \sin 2\psi \sin \Delta]$ are shown in Figure 4b. $\varepsilon_s = T_s$ and $\varepsilon_p = T_p$, the emission coefficients of s and p waves, are shown in Figure 4c. $\mathbf{S_o}$ is the radiation from the interior of the target.

(a) ψ and Δ. (b) Mueller matrices. (c) ε_s and ε_p.
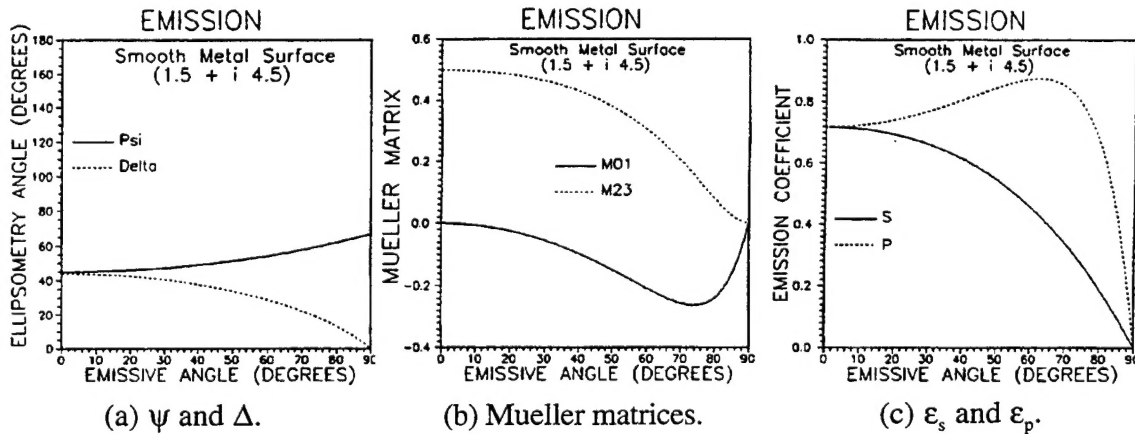
FIGURE 4. The Calculated Emission ψ, Δ, Mueller Matrix Elements and ε_s, ε_p for a smooth Metal Plane of Optical Constants $1.5 + i\,4.5$.

POLARIZATION IMAGES OF CYLINDRICAL SURFACE
NEAR A WATER PLANE

In this section we calculate the polarization images of a model target with a cylindrical surface. As shown in Figure 5, the cylinder is near and parallel to a water plane. Since the emissive circular radiation from cylindrical surface is negligibly small, we consider only the cases in which the light is either (1) emitted or (2) reflected from the water plane and then reflected from the cylinder toward the sensor (References 3 and 4). xyz are the target coordinates and the observer imager coordinates are XYZ. x'y'z'-axes [z'=z] are chosen such that the x'-axis is normal to the water plane [y'z'-plane]. In addition to the aspect angle θ_a, the observer direction has an azimuthal angle δ_a.
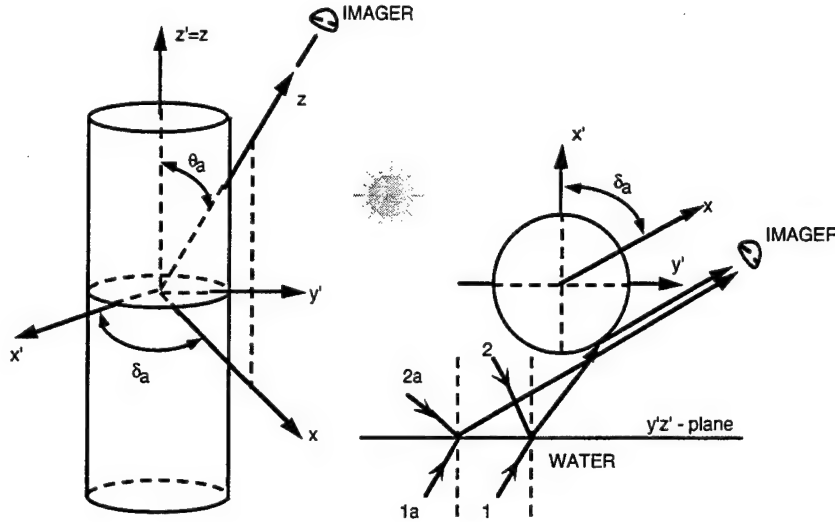
FIGURE 5. The Observation Geometry of a Cylinder Above the Water Plane.

The observed emission/reflection radiation from the cylinder (Ray 1 of Figure 5) is

$$\mathbf{S} = \mathbf{M}_{re} \mathbf{S}_o, \tag{7}$$

where $\mathbf{M}_{re} = \mathbf{R}(\Theta_{ot}) \mathbf{M}_r \mathbf{R}(\Theta_{tp}) \mathbf{M}_e$ (8)

is the resultant Mueller matrix associated with the radiation emitted from the dielectric plane and then reflected from the cylindrical surface (Reference 4). $\mathbf{S}_e [= \mathbf{M}_e \mathbf{S}_o]$ is the emission from the water plane toward the cylinder. $\mathbf{M}_r$ is the reflection at the cylindrical surface. Θ_{tp} is the angle between the two s-axes of the target and plane surfaces. Θ_{ot} is the angle between the imager X-axis and the s-axis of the reflecting target surface.

$$\text{where} \quad \mathbf{R}(\Theta) = \begin{pmatrix} 1 & 0 & 0 & 0 \\ 0 & \cos 2\Theta & \sin 2\Theta & 0 \\ 0 & -\sin 2\Theta & \cos 2\Theta & 0 \\ 0 & 0 & 0 & 1 \end{pmatrix} \tag{9}$$

Taking $\mathbf{S}_o = (1, 0, 0, 0)$, then $\mathbf{S}_e = (\varepsilon_I, \varepsilon_Q, \varepsilon_U, \varepsilon_V)$ and $\mathbf{S} = (\varepsilon R_I, \varepsilon R_Q, \varepsilon R_U, \varepsilon R_V)$. εR_I, εR_Q, εR_U, εR_V are the effective emissivity-reflectance, due to the emission and reflection from the two surfaces, for I, Q, U, and V components respectively. Taking the metal surface of optical constants $1.5 + i\,4.5$, and 10 degrees for the aspect angle, the images are calculated for $\delta_a = 70$ degrees. The results are shown in Figure 6.

The reflection image field in the Y-direction is reduced because of the emission-reflection geometry. The $[\varepsilon R]_j$ images of the target are in the region $Y/r < 1$. $Y/r > 1$ is the imaging region that shows the emissivities ε_j ($j = I, Q, U, V$) of water surface (Ray 1a of Figure 5). In this case we find that significant circular polarization signature exists. εR_V has a maximum value 0.06. These results show that the circular polarization signature of a target due to reflection is not always small and thus cannot be neglected. Therefore, it is potentially useful for practical applications.
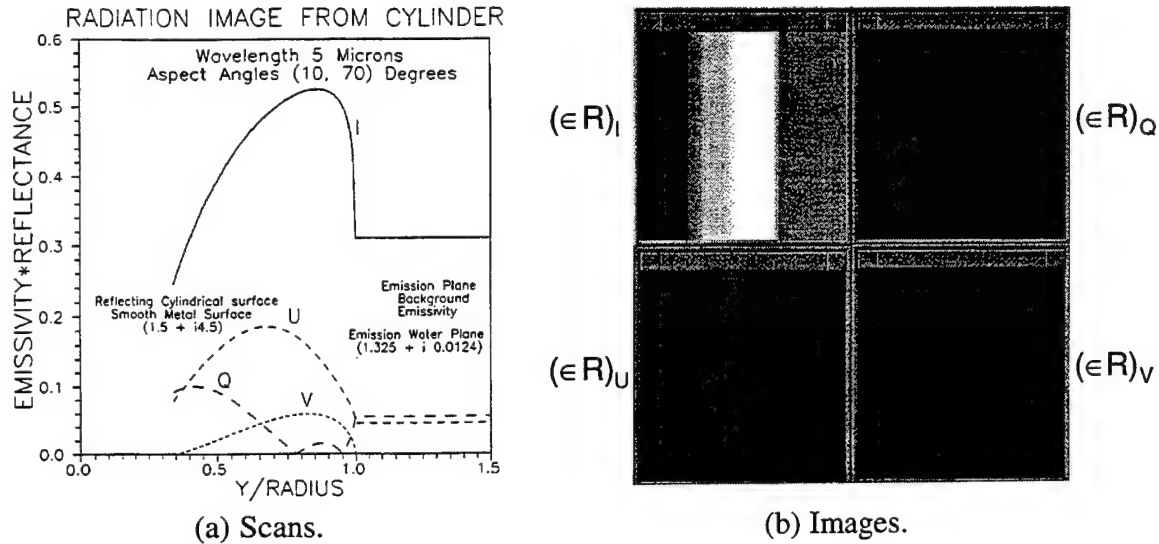

(a) Scans.   (b) Images.

FIGURE 6. Calculated Scans and Images of Emissivity-Reflectance From a Metal Cylindrical Target Surface ($0 < y/R < 1$) and Emissivity of the Emissive Water Plane ($1 < y/R < 1.5$) Observed at $\theta_a = 10$ Degrees and $\delta_a = 70$ Degrees and Wavelength 5 Micrometers.

Similarly, the observed reflection/reflection radiation from the cylinder (Ray 2 of Figure 5) is

$$\mathbf{S} = \mathbf{M}_{rr}\mathbf{S}_0, \tag{10}$$

where $\mathbf{M}_{rr} = \mathbf{R}(\Theta_{ot})\,\mathbf{M}_r\,\mathbf{R}(\Theta_{tp})\,\mathbf{M}_r$ $\tag{11}$

is the resultant Mueller matrix associated with the radiation reflected from the water plane and then reflected from the cylindrical surface (Reference 4). $\mathbf{S}_r\,[=\mathbf{M}_r\,\mathbf{S}_0]$ is the reflected signal from the water plane toward the cylinder (Ray 2a of Figure 5).

POLARIZATION EMISSION-REFLECTION SIGNATURE OF A CYLINDRICAL TARGET ABOVE A FLAT WATER PLANE

For a target at a long range where the emission image becomes a point source and may be contained within one pixel of the focal plane array, the total radiant intensities toward the sensor pixel are

$$I_j = \int dS_n \int_{\lambda_{min}}^{\lambda_{max}} d\lambda\, \varepsilon_j(\lambda,T)\, L_B(\lambda,T) \tag{12}$$

where $j = I, Q, U, V, L_B(\lambda,T) = \dfrac{2hc^2}{\lambda^5} \dfrac{1}{\exp(hc/\lambda k_B T)-1}$ is the blackbody radiance function. ε_j and T are the emissivity and absolute temperature of the target/debris surface toward the sensor. $[\lambda_{min},\lambda_{max}]$ is the waveband. ε_j is replaced by R_j in the reflectance case, or $[\varepsilon R]_j$ and $[RR]_j$ in the emission-reflection and reflection-reflection cases respectively. For the target at range Rg, the irradiance onto the sensor is $E_j = \dfrac{I_j}{R_g^2}$. If we neglected the atmospheric absorption, the acquisition ranges would be

$$\left[R_g\right]_j = \left[\frac{I_j}{E_m}\right]^{1/2} \tag{13}$$

E_m is the minimum detection irradiance (MDI) of the sensor.

Figure 6 shows that the I-, Q-, and U- images of emissive water background are nonvanishing, with magnitudes comparable to those of the emission-reflection radiation from the target, and will have a serious target signal-clutter contrast problem. However, negligible V-signature exists from the water background, and then there is no signal-clutter contrast problem for the circular polarization V-image. This result has clearly demonstrated the potential benefit for sea-skimming missile detection using the circular polarization. The criterion is that the target's V-signature must be strong and detectable by the infrared sensors. To show the feasibility, a model calculation has been performed and is described in the following paragraphs.

We consider a cylindrical target model 10 meters long, 0.5 meters radius, and 10 meters above a water plane (XY-plane) as shown in the Figure 7. This model is located at a distance 20 kilometers from the YZ-plane and with its axis in the XZ-plane and along the X-direction. The sensor is located in the YZ-plane and with a distance 3.5 kilometers from the XZ-plane and an altitude 1.27 kilometers above the water surface. This geometry gives $\theta_a = 10$ and $\delta_a = 70$ degrees. Assuming that the target surface is made from a stainless-steel-like metal with optical constants $1.5 + i\,4.5$ and the water temperature is 286 K and with optical constants $1.325 + i0.0124$ (at a wavelength of 5 micrometers), the water-background emissivity-reflectance $[\varepsilon R]_j$ scans are shown in Figure 6.

For the case of $\delta_a = 70$ degrees, the θ_a-dependent emission-reflection MWIR (wavelength 4.7 - 5.3 micrometers) radiant intensities towards the sensor are shown in Figure 8. For a MDI, $E_m = 10$ fW/cm^2, the acquisition ranges are calculated, using Equation 13 and are also shown in Figure 8. The target V-signature at $\theta_a = 10$ and $\delta_a = 70$ degrees is observable with respect to the negligible water background. This result has provided the foundation for the application of circular polarization to the problem of a sea-skimming missile detection for ship-defense.
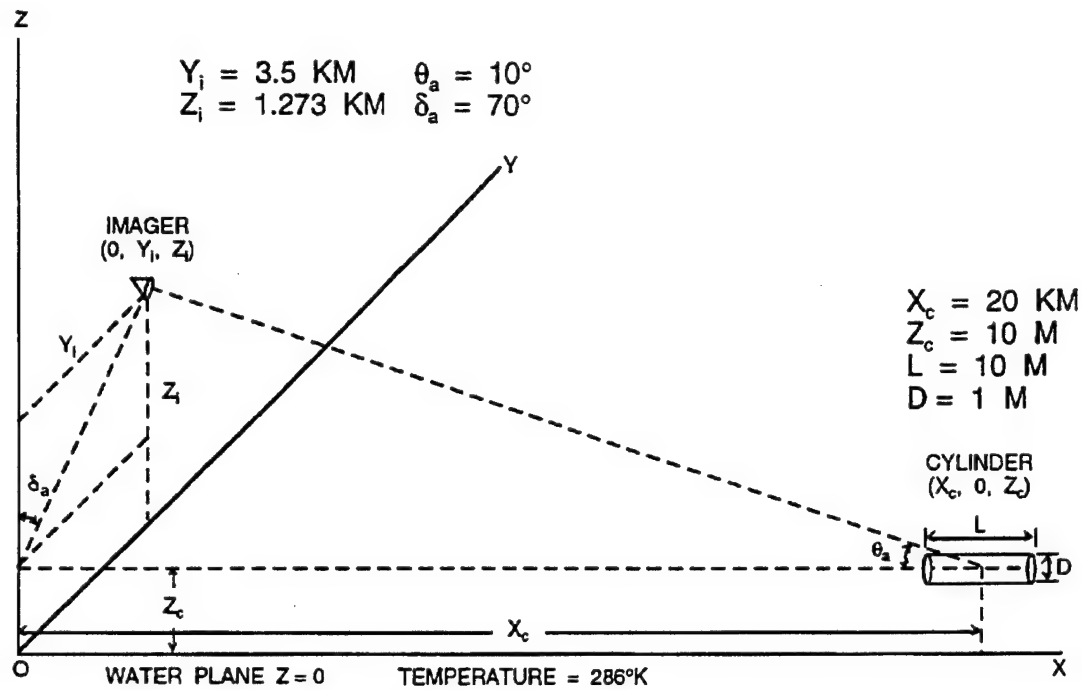
FIGURE 7. A Model Geometry of the Imaging Sensor and a Cylindrical Target Above a Flat Water Plane.
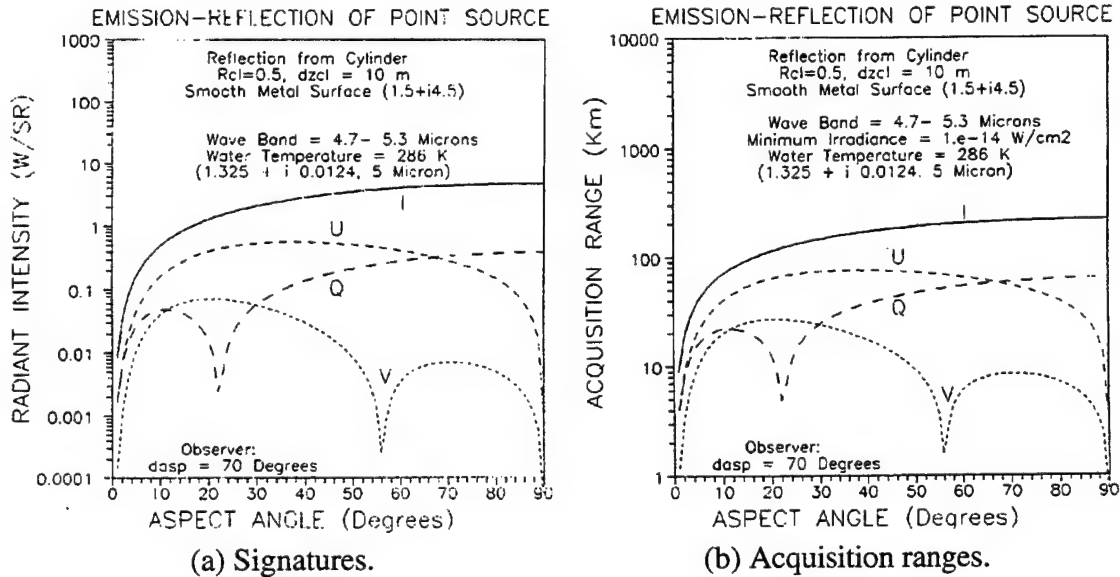

(a) Signatures.

(b) Acquisition ranges.

FIGURE 8. The MWIR (Waveband 4.7 - 5.3 Micrometers) Stokes Parameter Emission-Reflection Radiant Intensities and Acquisition Ranges (MDI = 10 fW/cm^2) of the Model Cylindrical Target With Optical Constants 1.5 + i 4.5, for Water Temperatures 286 K.

CIRCULAR POLARIZATION REFLECTION-REFLECTION SIGNATURE OF A CYLINDRICAL TARGET ABOVE A SEA SURFACE IN SOLAR CORRIDOR

We generalize the concept and model to study the detection of a sea-skimmer in the solar corridor. In the model calculation, we consider only the major solar radiation source and neglect other radiation contributions. The effects of (1) the atmospheric absorption and (2) the rough sea surface are included. The atmospheric absorption and the solar radiation spectra have the major effect for band selection. The rough water surface would produce nonvanishing circular background. These effects are negligible in the flat surface case. As shown in Figure 5 [ray 2], the total intensity of the cylindrical skimmer toward the sensor is

$$I_j = \int dS_n \int_{\lambda_{min}}^{\lambda_{max}} d\lambda \left[RR_w \right]_j W_s(\lambda, T_s)/\Omega_s \tag{14}$$

where $T_s = 6000$ K is the solar temperature, $W_s(\lambda, T_s)$ is the solar spectral irradiance at sea surface and is shown in Figure 9 for the MWIR band (Reference 9). $[RR_w]_j$ are the effective reflectance coefficients due to the double reflections of water $[R_w]$ and missile surface $[R]$. $\Omega_s = 6.3E-3$ str is the solid angle of solar disk. For the target at range Rg, the irradiance onto the sensor is

$$E_j = \tau(R_g) \frac{I_j}{R_g^2} \tag{15}$$

$\tau(R_g)$ is the spectrally $[\lambda_{min}, \lambda_{max}]$ averaged atmospheric transmission coefficient between the target and the sensor.

The total radiant intensity of the water-reflected solar radiation toward the sensor is

$$I_{wj} = \int dS_n \int_{\lambda_{min}}^{\lambda_{max}} d\lambda \left[R_w \right]_j W_s(\lambda, T_s)/\Omega_s \tag{16}$$

$[R_w]_j$ is the effective reflectance coefficient of water surface. For the water surface at range R_g, the irradiance onto the sensor (ray 2a of Figure 5) is

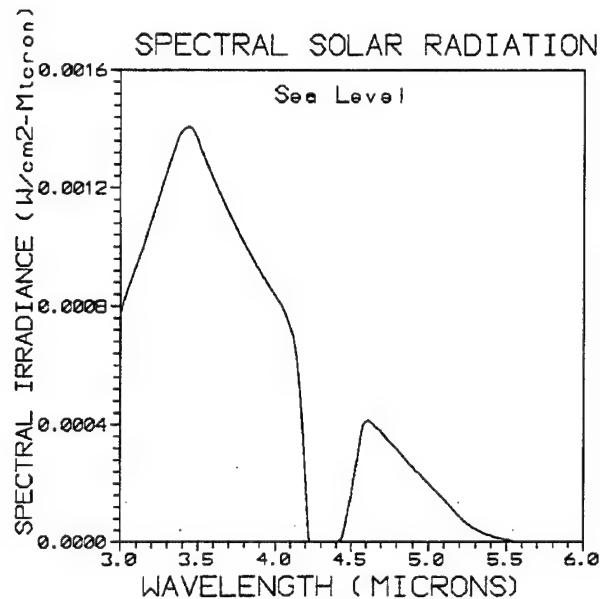$$E_{wj} = \tau(R_g) \frac{I_{wj}}{R_g^2} \tag{17}$$

FIGURE 9. The MWIR Solar Spectral Irradiance at Sea Surface.

FLAT-WATER-PLANE MODEL

We consider a cylindrical target model 10 meters long, 0.5 meters radius, and 10 meters above a water plane (XY-plane) as shown in the Figure 7. This model is located at a distance X kilometers from the YZ-plane and with its axis in the XZ-plane and along the X-direction. The sensor at two positions is studied: (1) a shipboard sensor located in the YZ-plane, at a distance 100 meters from the XZ-plane and an altitude 20 m above the water surface and (2) an interceptor helicopter-board sensor located in the YZ-plane, at a distance 2 km from the XZ-plane and an altitude 1 kilometer above the water surface. The situation is shown in Figure 10.

We assume that the water-reflected solar glint toward the sensor has a spread incident angles of (1) 10-degree range (79.95 to 89.95 degrees) and (2) 40-degree range (49.95 to 89.95 degrees), respectively. We also assume that the target surface is made from a painted surface with optical constants $1.5 + i\,0.15$, and the water has optical constants $1.374 + i0.0036$, (at a wavelength of 3.7 micrometers) (Reference 10).

For the case of flat water surface, the irradiances of I-, V-, and water background I-signatures (MWIR band 3.4 - 4.0 micrometers) are calculated and shown in Figure 11. In this geometry, the strong water-reflected solar glint exists for a horizontal range X > 2 kilometers. In this solar corridor, the target I- irradiance is much smaller than the water-reflected solar I-background. Taking the sensor MDI = 10 fW/cm^2, the circular component target signatures are measurable and have acquisition ranges of 16.2 and 56.8 kilometers for positions 1 and 2, respectively. The band 3.3 to 3.7 micrometers is a near optimum choice of the greatest spectral signature of solar radiation source near the sea surface (Figure 9).

13

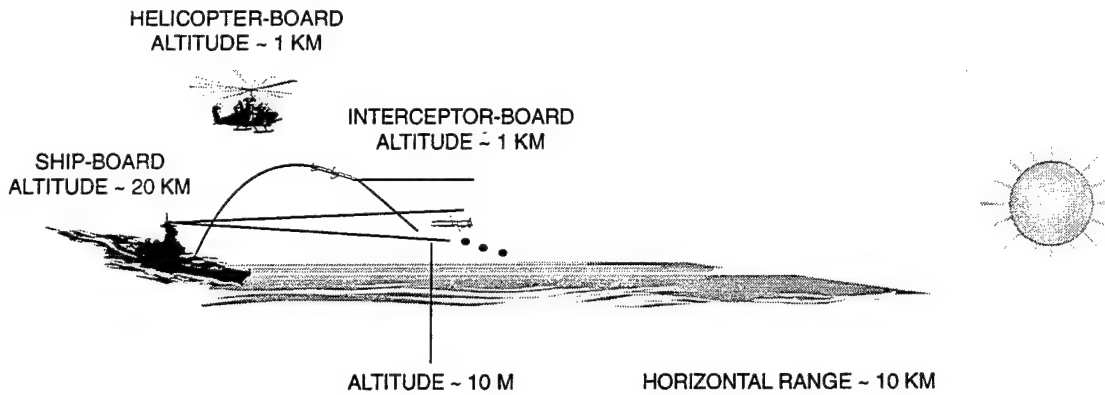FIGURE 10. Model Sensor Target Geometry in the Solar Corridor.

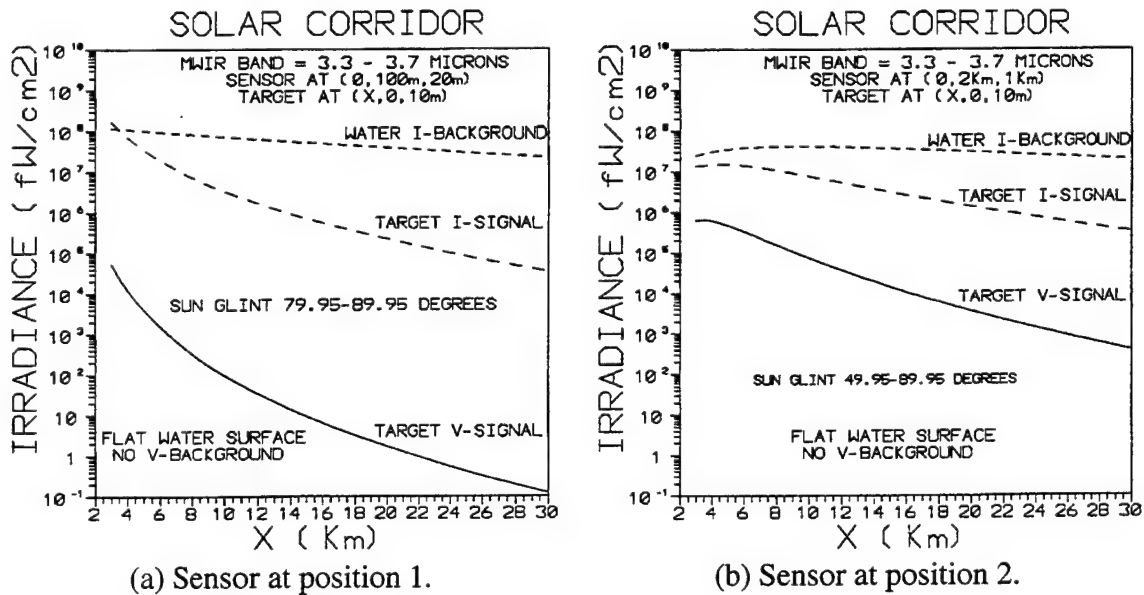(a) Sensor at position 1.

(b) Sensor at position 2.

FIGURE 11. The MWIR Irradiances of Solar Glints. The sensors are at (1) [0, 100 m, 20 m] and (2) [0, 2 km, 1 km]. Flat water surface is assumed.

ROUGH-SEA-SURFACE MODEL

The double reflection of unpolarized solar radiation from two surfaces would generate circular component radiation with a nonvanishing V signature. Then the nonvanishing V-component of rough-sea background is expected. This effect will limit the application potential of sea-skimmer detection in the solar corridor. We make a study of the strength.

A model based upon double reflection (Reference 11) for a rough-surface backscattering was developed (Reference 12). In this model, the polarization properties of double-reflection surface scattering (effective Mueller matrix) are derived. Using the sea-surface slope distribution of Cox-Munk model, the Mueller matrix and the MWIR (I, Q, U, V) signatures of the reflected solar background from a rough-water surface are calculated. The degrees of circular (V/I) and linear (I_{lp}/I) polarizations are calculated (Reference 13). The results for the near grazing cases (incident angles greater than 80 degrees) for sea surfaces with wind speeds of 0, 2.5, 5, and 10 m/s are shown in Figure 12. Figure 12 shows that the circular polarization signal (V) is less than 1E-6 of the intensity signal (I) near the horizon (incident angle > 89 degrees).

For the two sensors at positions 1 [0, 100, 20 meters] and 2 [0, 2, 1 kilometers], the I-, V-irradiances of target and water background [MWIR band 3.3 to 3.7 micrometers] are calculated. The results for sea-surface wind speeds of 0 and 10 m/s are calculated and shown in Figures 13 and 14. The ratio E_V/E_{Vw} is calculated and also shown in Figure 15.

The relation E_V/E_{Vw} versus E_V for the sensor at position 1 are shown in Figure 16. If we take the sensor MDI to be 10 fW/cm^2, the acquisition ranges of sensor 1 are 9.9 and 7.7 kilometers for sea surfaces with wind speeds 0 and 10 m/s respectively. At these ranges the circular polarization signal-to-clutter ratios, E/E_w, are 76 and 330 respectively. Therefore, the circular component clutter background (E_w) due to roughness of sea surface is negligibly small. The relation E_V/E_{Vw} versus E_V for the sensor at position 2 is shown in Figure 17.

The circular sea background E_w is large. Taking E/E_w = 10 as the range criterion, the acquisition ranges are 13.9 and 11.5 kilometers for sea surface with wind speeds 0 and 10 m/s respectively. At these ranges the circular polarization target irradiance E is 2700 and 1445 fW/cm^2 respectively. The results are listed in Table 1.

The circular component target signature (E) is very strong. These results show that the MWIR circular polarization sensor is feasible for the sea-skimming missile detection in the solar corridor, either for (1) shipboard or (2) interceptor/helicopter-board sensor application. The range of ship defense interest is 7 to 14 kilometers.
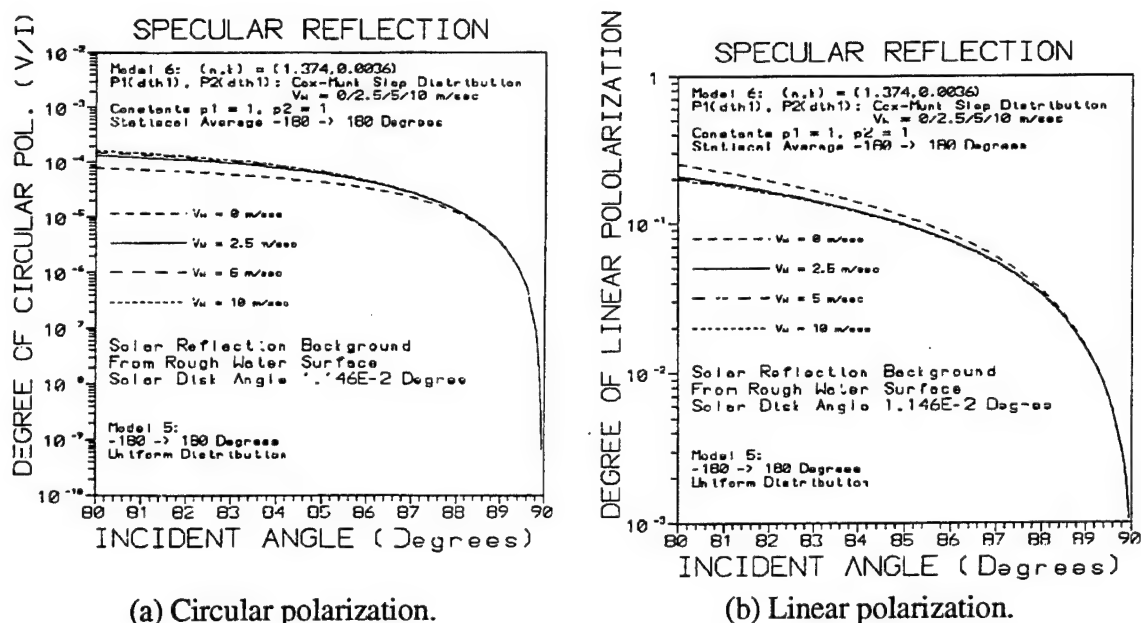
SPECULAR REFLECTION

Model 6: (n,t) = (1.374,0.0036)
P1(dth1), P2(dth1): Cox-Munk Slop Distribution
Vu = 0/2.5/5/10 m/sec
Constants p1 = 1, p2 = 1
Statiscal Average -180 -> 180 Degrees

- - - - - Vu = 0 m/sec
─────── Vu = 2.5 m/sec
- - - - Vu = 5 m/sec
.... Vu = 10 m/sec

Solar Reflection Background
From Rough Water Surface
Solar Disk Angle 1.146E-2 Degree

Model 5:
-180 -> 180 Degrees
Uniform Distribution

DEGREE OF CIRCULAR POL. (V/I) — **INCIDENT ANGLE (Degrees)**

(a) Circular polarization.

SPECULAR REFLECTION

Model 6: (n,t) = (1.374,0.0036)
P1(dth1), P2(dth1): Cox-Munk Slop Distribution
Vu = 0/2.5/5/10 m/sec
Constants p1 = 1, p2 = 1
Statiscal Average -180 -> 180 Degrees

- - - - - Vu = 0 m/sec
─────── Vu = 2.5 m/sec
- - - - Vu = 5 m/sec
.... Vu = 10 m/sec

Solar Reflection Background
From Rough Water Surface
Solar Disk Angle 1.146E-2 Degree

Model 5:
-180 -> 180 Degrees
Uniform Distribution

DEGREE OF LINEAR POLOLARIZATION — **INCIDENT ANGLE (Degrees)**

(b) Linear polarization.

FIGURE 12. Polarization Background of Water Reflection. The degrees of circular (V/I) and linear (I_{lp}/I) polarizations for the near grazing cases with incident angles greater than 80 degrees. Results for sea surfaces with wind speeds of 0, 2.5, 5, and 10 m/s (Cox-Munk model) are shown.

SOLAR CORRIDOR

MWIR BAND = 3.3 - 3.7 MICRONS
SENSOR AT (0,200m,20m)
TARGET AT (X,0,10m)

WATER I-BACKGROUND

TARGET I-SIGNAL

COX-MUNK SEA SLOPE MODEL
WIND SPEED = 0 m/Sec

SUN GLINT 79.95-89.95 DEGREES

TARGET V-SIGNAL

WATER
V-BACKGROUND

IRRADIANCE (fW/cm2) — **X (Km)**

(a) Wind speed 0 m/s.

SOLAR CORRIDOR

MWIR BAND = 3.3 - 3.7 MICRONS
SENSOR AT (0,200m,20m)
TARGET AT (X,0,10m)

WATER I-BACKGROUND

TARGET I-SIGNAL

COX-MUNK SEA SLOPE MODEL
WIND SPEED = 10 m/Sec

SUN GLINT 79.95-89.95 DEGREES

TARGET V-SIGNAL

WATER
V-BACKGROUND

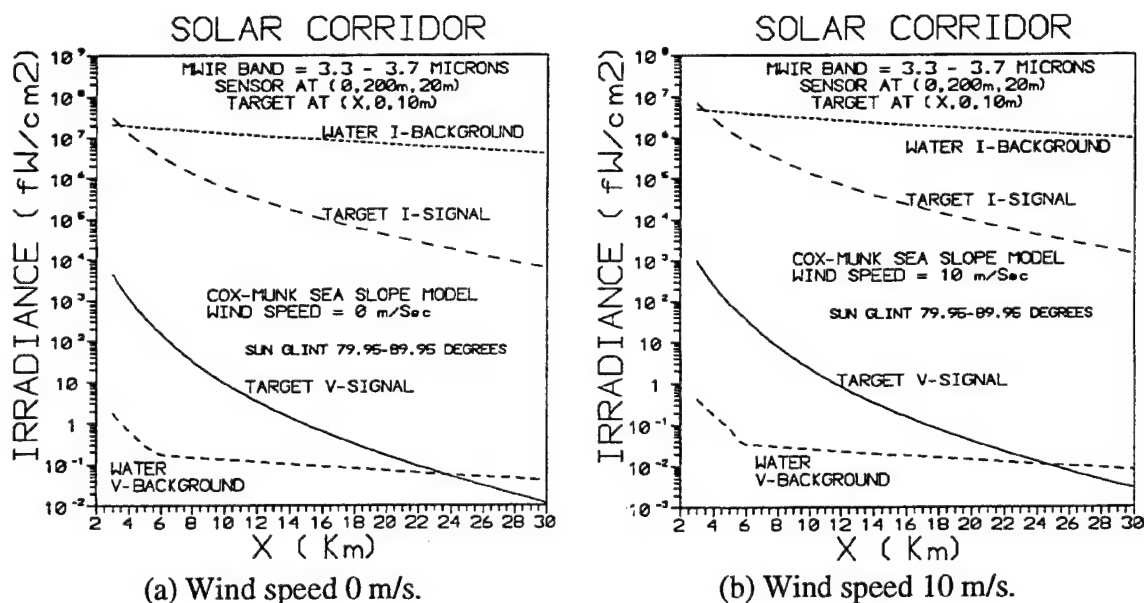**IRRADIANCE (fW/cm2)** — **X (Km)**

(b) Wind speed 10 m/s.

FIGURE 13. For the Sensor at Position 1, the MWIR Solar Glints Generated I- and V-Irradiances of the Model Cylindrical Target, and That of Water Background in Solar Corridor. Results for sea surfaces with wind speeds of 0 and 10 m/s (Cox-Munk model) are shown.

(a) Wind speed 0 m/s.
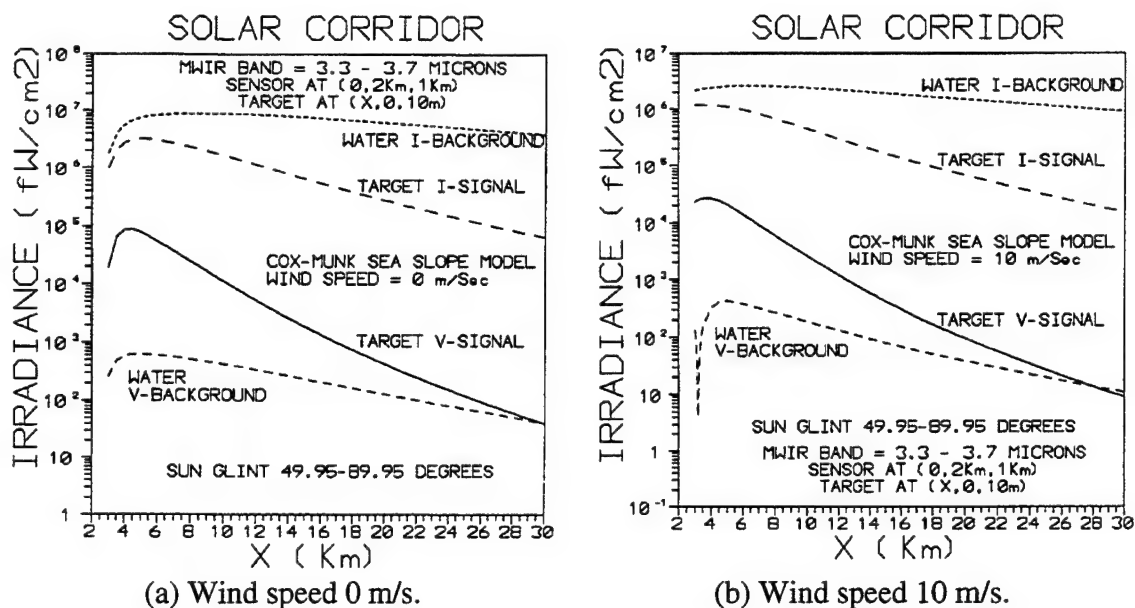
(b) Wind speed 10 m/s.

FIGURE 14. For the Sensor at Position 2, the MWIR Solar Glints Generated I- and V-Irradiances of the Model Cylindrical Target, and That of Water Background in the Solar Corridor. Results for sea surfaces with wind speeds of 0 and 10 m/s (Cox-Munk model) are shown.
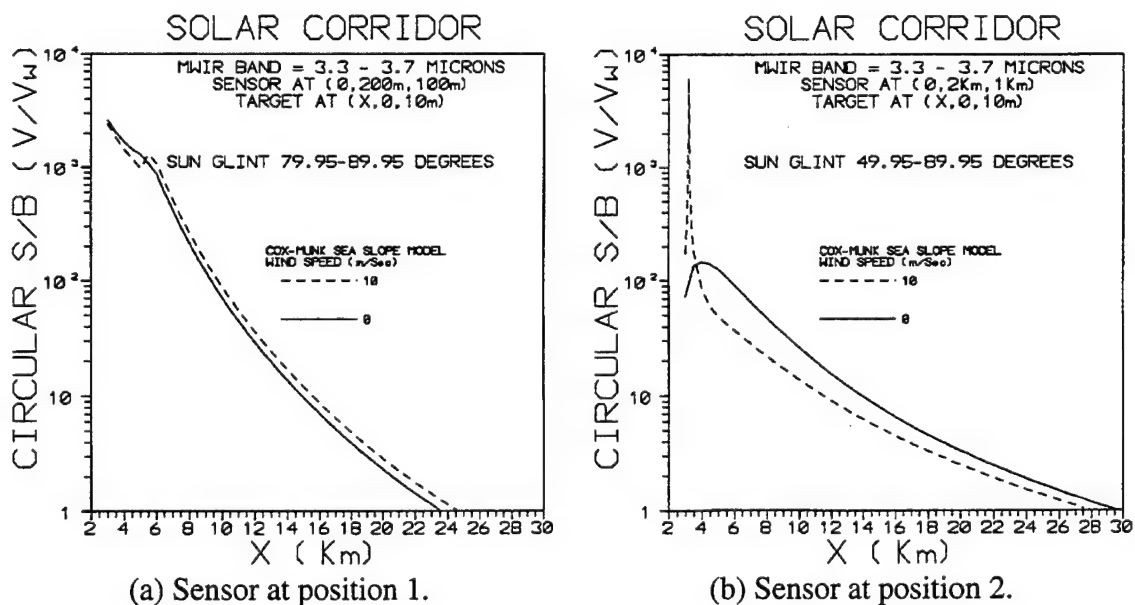

(a) Sensor at position 1.

(b) Sensor at position 2.

FIGURE 15. For the Sensor at Positions 1 and 2 and in the Solar Corridor (Figures 13 and 14), the Circular Polarization Signal to Clutter Ratio V/V_w.
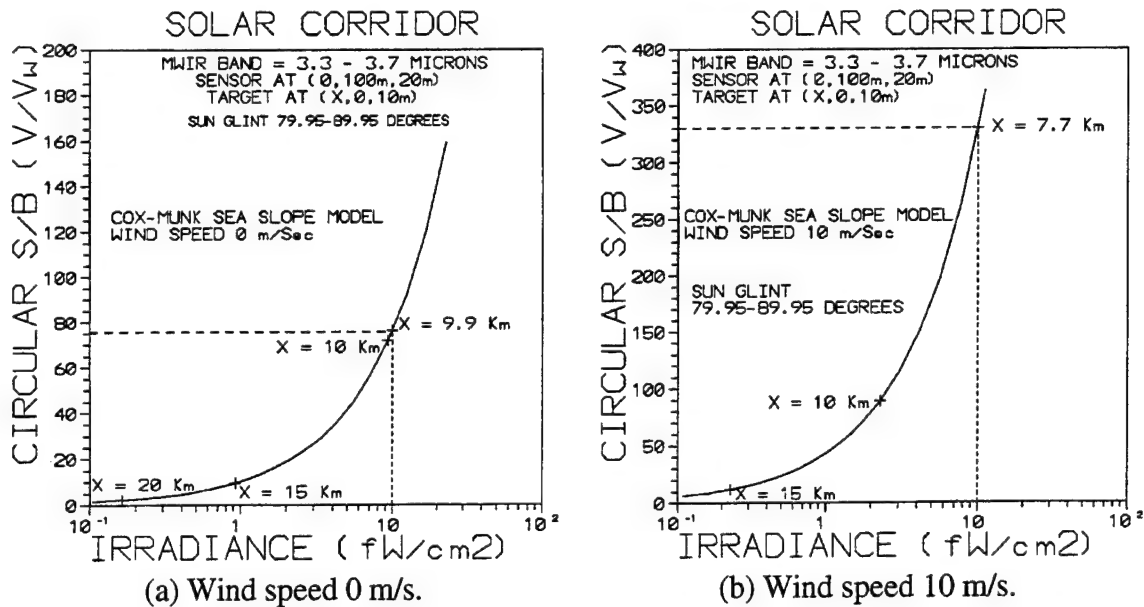
(a) Wind speed 0 m/s.

(b) Wind speed 10 m/s.

FIGURE 16. The E_V/E_{Vw} Versus E_V Relation for the Sensor at Position 1. The horizontal ranges X are marked.

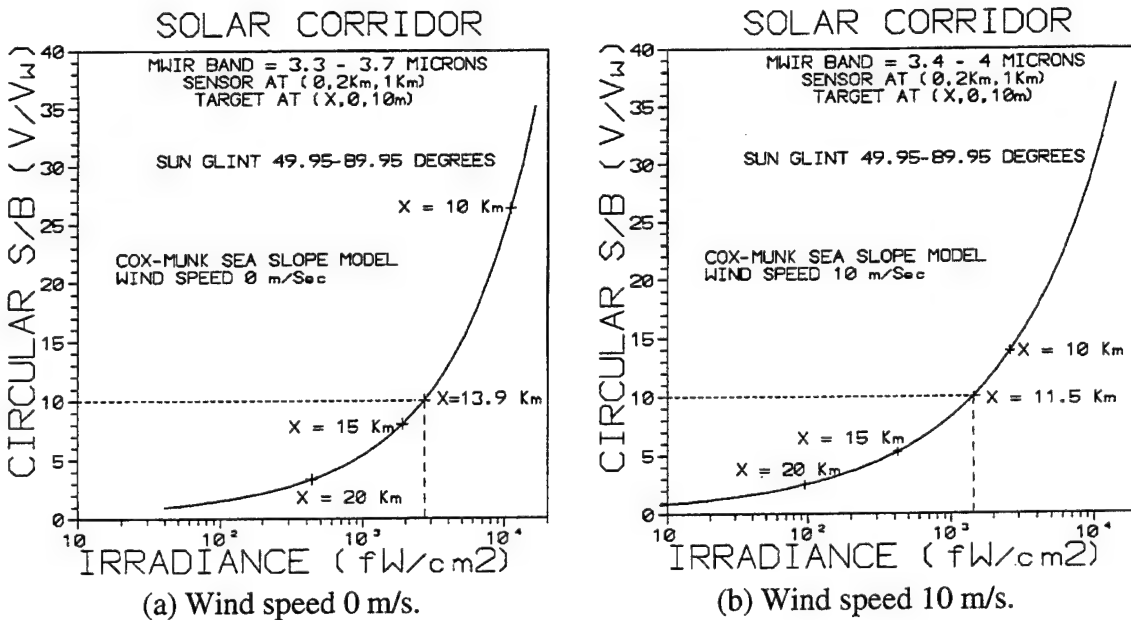(a) Wind speed 0 m/s.

(b) Wind speed 10 m/s.

FIGURE 17. The E_V/E_{Vw} Versus E_V Relation for the Sensor at Position 2. The horizontal ranges X are marked.

TABLE 1. Acquisition Ranges for the Two Sensors
at Positions 1 and 2.

Parameter	Position	Wind speed (m/s)	
		0	10
Acq. range (km)	1	9.9	7.7
	2	13.9	11.5
E (fW/cm^2)	1	10	10
at acq. range	2	2700	1445
E/E$_w$	1	76	330
at acq. range	2	10	10

DISCUSSION AND CONCLUSIONS

We calculated the polarization signatures of a model cylindrical target with painted surface. The circular polarization reflection-reflection signatures for the cylinder above water plane with both flat and rough (Cox-Munk model, Reference 13) sea surface are studied quantitatively. The result shows the feasibility of detecting sea-skimmer targets above the sea surface. In the solar corridor, the sun glints reflected from the water surface and then reflected from a target surface would have significant circular polarization. These reflected sun glints are stronger than the reflection background from rough sea surface (Figure 15). Therefore, a circular polarization sensor would be feasible to work as an adjunct sensor for sea-skimming missile detection in the solar corridor when the current intensity-only sensor has difficulty.

We consider two sensor positions, (1) shipboard and (2) interceptor helicopter-board sensor, which are the major interest of naval ship defense application. Until now no circular polarization imaging sensor has existed. The research and development of circular polarization sensor technology is a challenge.

For the night application without a hot solar source the thermal radiation emitted from the sea surface and then reflected from the target could also produce the circular polarization signature for discrimination and tracking. The long-wave infrared (LWIR) is preferred because of the low water temperature of the sea. Therefore, band selection is a key consideration of circular polarization sensor design for the special application environment.

The conclusions are the following:

1. Theory and algebra of circular polarization of target signatures have been developed.

2. The circular component solar glint background reflected from rough sea surface is negligibly small.

3. A MWIR circular polarization sensor is feasible for sea-skimming missile detection in the solar corridor.

4. The best MWIR band has been simulated and determined.

5. Infrared circular polarization sensor technology is worthy of development.

REFERENCES

1. Hess, M. R., G. A. Freund, D. L. McMaster, D. B. Nichols, M. A. LeCompte, F. J. Iannarilli, and J. E. Rice. "Measurement and Analysis of Aircraft Infrared Signature Polarization," in *IRIA-IRIS Proceedings: 1994 Meeting of the IRIS Specialty Group on Targets, Backgrounds and Discrimination*, Vol. IV (September 1994), pp. 207-226.

2. Nee, Tsu-Wei, and Soe-Mie F. Nee. "Infrared polarization signatures for targets," *Proc. SPIE 2469*, April 1995, pp. 231-241.

3. Nee, T. W., J. Bevan, J. Bobinchak, and S. F. Nee. "Infrared Polarization Signatures for Target/Background," *Proceeding of Workshop on Infrared and Millimeter Wave Polarimetry 5-7 December 1995*. Redstone Arsenal, Ala., April 1996, pp. 163-181.

4. Nee, T. W., S. F. Nee and E. J. Bevan. "Infrared Polarization Signatures of a Target for Enhanced Discrimination," in *IRIA-IRIS Proceedings: 1996 Meeting of the IRIS Specialty Group on Targets, Backgrounds and Discrimination*. Vol. IV (October 1996), pp. 349-368.

5. Nee, T. W., S. F. Nee and E. J. Bevan. "Infrared Polarization Imaging Sensor for TBMD Discrimination and Tracking," *The Second Theater Missile Defense Critical Measurements Program Data Analysis Workshop Proceedings*. Vol. III, MIT Lincoln Laboratory, Massachusetts, 22-24 January 1997, pp. 1379-1399.

6. Cheng, L., and G. Reys. "AOTF Polarimetric Hyperspectral Imaging for Mine Detection," *Proc. SPIE 2496*, Orlando, Fla., April 1995, pp. 305-311.

7. Chun, C. S. L., D. L. Fleming, W. A. Harvey, E. J. Torok and R. D. Juday. "Polarization-Sensitive Thermal Imaging Sensor," *Proceeding of Workshop on Infrared and Millimeter Wave Polarimetry 5-7 December 1995*. Redstone Arsenal, Ala., April 1996, pp. 131-139.

8. Nee, T. W., S. F. Nee and E. J. Bevan. "Polarization Effects on MWIR Target Signature Prediction and Discrimination Applications," *IRIA-IRIS 1998 Meeting of the IRIS Specialty Group on Targets, Backgrounds and Discrimination.*, 27-29 January 1998, Tucson, Ariz.

9. Bell, E. E., L. Eisner, J. Young, R. A. Oetjen. "Spectral Radiance of Sky and Terrain at Wavelengths Between 1 and 20 Microns. II. Sky Measurements," *J. Opt. Soc.* Am **50,** pp. 1313-1320 (1960).

10. Nee, S. F., P. C. Archibald, J. M. Bennett, D. K. Burge, and T. W. Nee. "Polarization by Rough Painted Surfaces," *Proceeding of Workshop on Infrared and Millimeter Wave Polarimetry 5-7 December 1995.* Redstone Arsenal, Ala., April 1996, pp. 527-542.

11. Gu, Z. H., J. Q. Lu and M. M. Tehrani. "Enhanced Backscattering of Polarized Light at Vacuum/Dielectric Interfaces," *Optical Eng., 34,* June 1995, pp. 1611-1624.

12. Nee, T. W., and S. F. Nee. "Polarization Theory of Rough Surface Scattering," (In process.)

13. Cox, C., and W. Munk. "Measurement of Roughness of the Sea Surface From Photographs of the Sun's Glitter," *J. Opt. Soc.* Am **44,** pp. 838-850 (1954).

INITIAL DISTRIBUTION

7 Chief of Naval Research, Arlington
    Code 31, B. Junker (1)
    Code 312, Y. Park (1)
    Code 313
      N. Gerr (1)
      W. Stachnik (1)
      J. Buss (1)
    Code 351, J. Chew (1)
1 Naval Post Graduate School, Department of Physics, Monterey (A. Cooper)
2 Naval Research Laboratory, Washington
    Code 5621, M. Hess
    Code 6810, J. Killiany
1 Naval Surface Warfare Center, Dahlgren Division, Dahlgren (R. Horman)
1 Air Force Wright Laboratories, Advanced Guidance Division, Wright-Patterson Airforce Base (WL/MNG, R. Wehling)
2 Defense Technical Information Center, Fort Belvoir
1 Northrop Grumman Corp., ESID, Bethpage, NY (A. Gartenberg)
2 Nichols Research Corp., System Development and Evaluation Center, Huntsville, AL
    B. Barbour (1)
    D. McGauley (1)

ON-SITE DISTRIBUTION

4 Code 4BL000D, (3 plus Archives copy)
1 Code 4BT000D, T. Loftus
1 Code 4T4110D, L. Desandre
1 Code 4T4120D, T. Nee
1 Code 47GA00D, A. Marshal
1 Code 471700D, J. Bevan
1 Code 472E00D, D. Burdick